

## Article

## Novel magnetite nanoparticles coated with waste sourced bio-based substances as sustainable and renewable adsorbing materials

Giuliana Magnacca, Alex Allera, Enzo Montoneri, Luisella Celi, Damian E Benito, Leonardo G. Gagliardi, Daniel Osvaldo Mártire, Mónica C Gonzalez, and Luciano Carlos

*ACS Sustainable Chem. Eng.*, **Just Accepted Manuscript** • Publication Date (Web): 13 May 2014

Downloaded from <http://pubs.acs.org> on May 14, 2014

### Just Accepted

“Just Accepted” manuscripts have been peer-reviewed and accepted for publication. They are posted online prior to technical editing, formatting for publication and author proofing. The American Chemical Society provides “Just Accepted” as a free service to the research community to expedite the dissemination of scientific material as soon as possible after acceptance. “Just Accepted” manuscripts appear in full in PDF format accompanied by an HTML abstract. “Just Accepted” manuscripts have been fully peer reviewed, but should not be considered the official version of record. They are accessible to all readers and citable by the Digital Object Identifier (DOI®). “Just Accepted” is an optional service offered to authors. Therefore, the “Just Accepted” Web site may not include all articles that will be published in the journal. After a manuscript is technically edited and formatted, it will be removed from the “Just Accepted” Web site and published as an ASAP article. Note that technical editing may introduce minor changes to the manuscript text and/or graphics which could affect content, and all legal disclaimers and ethical guidelines that apply to the journal pertain. ACS cannot be held responsible for errors or consequences arising from the use of information contained in these “Just Accepted” manuscripts.



1  
2  
3 **Novel magnetite nanoparticles coated with waste sourced bio-based substances as**  
4 **sustainable and renewable adsorbing materials**  
5  
6

7 Giuliana Magnacca<sup>†</sup>, Alex Allera<sup>†</sup>, Enzo Montoneri<sup>†</sup>, Luisella Celi<sup>‡</sup>, Damián E. Benito<sup>§</sup>,  
8 Leonardo G. Gagliardi<sup>§</sup>, Mónica C. Gonzalez<sup>□</sup>, Daniel O. Mártire<sup>□</sup> and Luciano Carlos<sup>□,\*</sup>  
9  
10

11  
12 <sup>†</sup> Dipartimento di Chimica, Università di Torino, Via Giuria 7, Torino, Italy.

13 <sup>‡</sup> Università di Torino, DIVAPRA, via L. da Vinci 44, Grugliasco, Italy.

14 <sup>§</sup> LIDMA, Universidad Nacional de La Plata, Calle 1 y 47, La Plata, Argentina.

15  
16 <sup>□</sup> Instituto de Investigaciones Fisicoquímicas Teóricas y Aplicadas (INIFTA), CCT-La Plata-  
17 CONICET, Universidad Nacional de La Plata, Diag 113 y 64, La Plata, Argentina.  
18  
19

20  
21  
22 \* To whom correspondence should be addressed. (L. Carlos) Phone: +54 221 4257430. Fax:  
23 +54 221 4254642. E-mail: lcarlos@quimica.unlp.edu.ar. Postal address: Casilla de correo 16,  
24 sucursal 4 (1900), La Plata, Argentina.  
25  
26  
27

28  
29 (E.M.) present address: University of Foggia, STAR\*Integrated Research Unit, Via Gramsci,  
30 89-91, Foggia, Italy.  
31  
32

33  
34 **Abstract**

35 This study examines the possibility of using bio-based product isolated from urban solid  
36 wastes as a material for environmental technological applications. To this end, Fe<sub>3</sub>O<sub>4</sub>  
37 nanoparticles coated with different amounts of soluble bio-based products (SBO) were  
38 synthesized as low-cost nanoadsorbent for the removal of pollutants in wastewater. Particles  
39 of 10 nm diameter with Fe<sub>3</sub>O<sub>4</sub> core and SBO shell were obtained. The concentration of SBO  
40 employed in the synthesis had no effect on the size and structure of the NPs, but ruled the  
41 pH<sub>PZC</sub> and aggregation of the nanoparticles in water. The cationic dye crystal violet (CV) was  
42 used as a model pollutant to test the adsorption capacity of the nanoparticles. The results  
43 indicated that both the medium pH and NP dosage were significant parameters to enhance the  
44 removal of CV. The results contribute to the studies which show how wastes can become a  
45 source of revenue through the industrial exploitation of their chemical value.  
46  
47  
48  
49  
50  
51  
52  
53  
54

55 **Keywords:** nanoadsorbents; magnetite; wastewater remediation; urban biowastes; renewable  
56 feedstock; crystal violet.  
57  
58

## INTRODUCTION

Not always the conventional wastewater treatments are effective in the removal of pollutants from wastewater, in particular when pollutants belong to several classes and possess different behaviors. In cases like these, further treatments need to be exploited. The aim of this study is to investigate unusual materials as adsorbents in order to act together and/or assist other abatement techniques.<sup>1</sup> Adsorbent materials present also the advantage to avoid the appearance of secondary pollution (due to the application of traditional degradative methods that can lead to the formation of toxic intermediates).

In recent years, a wide number of publications have been dedicated to the removal of pollutants from wastewater by using adsorption techniques. One of the most important requirements to keep in mind during the development of these strategies is the cost of the technologies proposed which needs to be very limited. In this respect, low-cost materials from natural sources (natural clay minerals like montmorillonite, bentonite, sepiolite, vermiculite, and zeolites), industrial wastes (such as fly ash, blast furnace slag and sludge, black liquor lignin, red mud, and waste slurry) and agriculture residues have been considered.<sup>2-7</sup> Adsorbents deriving from agricultural operations, in particular, deserve a careful evaluation, since they are available in large quantities, are environmental friendly and have almost no costs.<sup>8</sup> In this context, the use of substances deriving from treatment of biowastes (green disposal and food) represents a good contribution to this research, and, to our best knowledge, solid urban wastes (or by-products) have never been tested as low-cost adsorbents. Recent research has shown that the recalcitrant lignin-like fraction of urban solid wastes is a cost-effective source of soluble bio-based product (SBO) that can be rather effective in a wide number of applications in the industry and environmental remediation.<sup>9-12</sup> SBO have been found to be mixtures of molecules differing in molecular weight (from 67 to 463 kg mol<sup>-1</sup>), composed of aliphatic C chains substituted by aromatic rings and several functional groups such as COOH, CON, CO, PhOH and O-alkyl among others.<sup>13</sup> Their potential use as adsorbent material for removal of pollutants from wastewater could be useful from a number of perspectives because it could contribute to reduce the environmental impact of urban wastes and it may revalorize solid urban wastes as a material of technological application.

This work takes inspiration from the preparation of magnetic materials using humic substances as active-adsorbing phase,<sup>14</sup> extending the study to the use of SBO extracted from wastes following an already optimized procedure.<sup>15</sup> In fact, in recent years, nanoscale iron oxides have attracted growing interest in water treatment and environmental remediation. In

1  
2  
3 particular, the use of magnetite nanoparticles as adsorbents in water treatment provides a  
4 convenient approach for separating and removing the contaminants by applying external  
5 magnetic fields. Since bare magnetite nanoparticles are susceptible to air oxidation and are  
6 easily aggregated in aqueous systems,<sup>16</sup> their surface modifications is commonly performed  
7 for its application as nanoadsorbent,<sup>17-19</sup>

8  
9  
10  
11 The present paper reports the preparation of Fe<sub>3</sub>O<sub>4</sub> nanoparticles (NPs) coated with  
12 SBO as low-cost nanoadsorbent for removal of pollutants in wastewater. The physical and  
13 chemical characterization of the synthesized SBO-coated Fe<sub>3</sub>O<sub>4</sub> nanoparticles was carried out.

14  
15  
16 Dye molecules when released to wastewaters cause serious environmental and health  
17 hazards.<sup>20</sup> In particular, the cationic azo dye crystal violet (CV) is considered a mitotic  
18 poison.<sup>21</sup> For these reasons and with the aim of developing a method for the removal of CV  
19 from waters, the sorption capacity of the SBO-coated Fe<sub>3</sub>O<sub>4</sub> nanoparticles for adsorbing the  
20 hazardous dye CV was tested and the effects of pH, ionic strength, and NPs dosages were  
21 evaluated.  
22  
23  
24  
25  
26

## 27 28 **EXPERIMENTAL**

### 29 *Synthesis*

30  
31 The coated magnetite nanoparticles were prepared by modifying the co-precipitation  
32 method in the presence of a suitable concentration of SBO. First, 3.7 g of FeCl<sub>3</sub> and 4.2 g of  
33 FeSO<sub>4</sub>·7H<sub>2</sub>O were dissolved in 100 mL of deionized water. The solution was brought to  
34 90°C, then 10 mL of NH<sub>4</sub>OH 25% and 50 mL of solution containing various amounts of SBO  
35 (0.05, 0.1 and 0.5 g) were sequentially added. The solution was kept at 90°C for 30 min under  
36 continuous stirring and subsequently cooled down to room temperature. The magnetic powder  
37 was separated from the basic solution using a laboratory magnet and washed three times with  
38 water in order to eliminate all the undesired soluble and non-magnetic products. Finally, the  
39 black powders were dried in a vacuum oven at 70°C for several hours and then stored at room  
40 temperature. Depending on the amount of SBO used during the synthesis (0.05, 0.1 and 0.5  
41 g), the samples were named as NP/0.05, NP/0.1 and NP/0.5, respectively.  
42  
43  
44  
45  
46  
47  
48

49 All commercial products used were purchased from Sigma Aldrich. The SBO  
50 employed in this study, namely CVT230, derived from 230 days composting of green refuse  
51 (at Acea Pinerolese plant at Pinerolo, Torino, Italy) and processed at the pilot plant of Studio  
52 Chiono e Associati at Rivarolo Canavese, Torino, Italy. The extraction procedure of CVT230  
53 as well as its physico-chemical characterization was already reported elsewhere.<sup>11,22</sup>  
54  
55  
56  
57  
58  
59  
60

### *Characterization*

Magnetization measurements were carried out with a LakeShore 7404 vibrating sample magnetometer. The hysteresis loop of the samples was registered at room temperature (25 °C) as the magnetic field was cycled between -2 and 2 kOe. Nitrogen adsorption at 77 K was followed using the gas-volumetric apparatus ASAP2020 by Micromeritics to determine specific surface area and porosity. Samples were pretreated for several hours at 70 °C in order to remove undesired atmospheric gaseous contaminants adsorbed on powders surface and/or pores. In some cases, powders were preliminary sonicated for 30 min in order to evaluate the presence (and stability) of particle aggregates. X-Ray Diffraction (XRD) patterns were obtained using PW3040/60 X'Pert PRO MPD diffractometer by PANalytical, equipped with Cu K $\alpha$  source, Bragg-Brentano geometry, in flat or capillary sample-holder, 10.240 sec/step with 2 $\theta$  steps of 0.01, in the 2 $\theta$  range 5-70°. The average crystallite size was estimated using the Scherrer equation. For the calculation, three diffraction peaks with the highest intensities were selected and the reported size values were the average of the results obtained for each peak. High-resolution Transmission Electron Microscopy (HRTEM) measurements were performed on a Jeol JEM 3010 UHR microscope (300 kV acceleration, LaB6 filament) equipped with a Digital image acquisition GATAN (2k x 2k) and EDS microanalysis (Oxford INCA ENERGY TEAM 200). Thermal gravimetric and differential thermal analysis (TGA-DTA) was performed with a TA Instruments TGA Q600 unit. Sample treatments were carried out in flow of air or nitrogen and the thermal program was: stabilization at 40 °C, heating (in flow of air or nitrogen) at 500 or 800 °C using a ramp rate of 10 °C min<sup>-1</sup>, maintaining at 500 or 800 °C for 10 min, and cooling down to room temperature. Fourier transform infrared (FTIR) spectra were recorded on a Bruker IFS 88 transmission spectrophotometer equipped with Globar source and DTGS detector. The resolution used was 4 cm<sup>-1</sup> with 128 scans in the range 4000-400 cm<sup>-1</sup>. KBr pellets were used (sample concentration 5% w/w). Acid-base titrations were done with a Schott Titroline Alpha titrator, equipped with a 20-mL burette syringe and connected to a Schott BlueLine 11-pH glass combination electrode. The system was controlled using Pyrator software. The end points of the titration curves were determined from the maximum on the first derivative curve. The pKa values were obtained from the minimum values of the first derivate of the pH curve. Reported results for each sample are the statistical average of at least three replicates. Particle size ( $d_z$ ) and zeta potential ( $\zeta$ ) were measured on the aqueous dispersions of magnetite nanoparticles by a Laser Doppler

1  
2  
3 Velocimetry coupled with Photon Correlation Spectroscopy using a Coulter DELSA 440  
4 spectrometer equipped with a 5 mW He-Ne laser (632.8 nm). Hydrodynamic diameters were  
5 deduced using the Stokes–Einstein equation and employing the particle diffusion coefficients  
6 calculated from the Doppler shift arising from Brownian motion. The electrophoretic mobility  
7 was calculated from the measurement of the Doppler shift for particles subjected to an electric  
8 field and these data were further converted to  $\zeta$  using the Smoluchowski equation.<sup>23</sup> All  
9 measurements were run in duplicate.  
10  
11  
12  
13  
14  
15

### 16 *Sorption Experiments*

17  
18 To evaluate the absorption ability of SBO-bonded Fe<sub>3</sub>O<sub>4</sub> nanoparticles, the adsorption  
19 of crystal violet (CV) was investigated in aqueous solutions at 25 ± 0.2 °C. In a typical  
20 removal procedure, SBO-coated Fe<sub>3</sub>O<sub>4</sub> nanoparticles were added into 200 mL of CV solution  
21 (10 mg L<sup>-1</sup>). The concentrations of the NPs ranged from 0.1 to 2 g. The solution pH was  
22 adjusted by NaOH or HCl to the desired value. The mixture was stirred in a closed beaker for  
23 3 h. Then the magnetic nanoparticles with sorbed CV were separated from the mixture with a  
24 permanent hand-held magnet. The residual CV concentration in the solution was determined  
25 spectrophotometrically using a double-beam Shimadzu UV/vis spectrophotometer. The effect  
26 of pH on the shape of the spectra was examined to avoid a misinterpretation of the  
27 spectrophotometric determinations at different pHs. For achieving the adsorption isotherms of  
28 CV, solutions with various initial dye concentrations were treated with the same procedure as  
29 above at room temperature (25 ± 0.2 °C). Every experiment was performed in triplicate and  
30 average values were used in the graphs.  
31  
32  
33  
34  
35  
36  
37  
38  
39

40 In this study all safety and environmental considerations have been taken into account.  
41 The chemical residues were disposed for further processing.  
42  
43  
44

## 45 **RESULTS AND DISCUSSION**

### 46 *Morphology and structure*

47  
48 Figure 1 shows representative TEM images of the nanoparticles NP/0.5 dispersed in  
49 aqueous medium. The particles appeared to be roughly spherical in shape, with a crystalline  
50 core and an external layer of organic matter. No significant differences were observed among  
51 the samples with different amounts of SBO (data not shown), except for the presence of the  
52 amorphous layer around the particles which is never visible for samples NP/0.1 and NP/0.05.  
53 The analysis of the TEM images revealed an average particle size of 10.2 ± 1.7 nm (Figures  
54  
55  
56  
57  
58  
59  
60

1  
2  
3 S1, Supporting information). This value is slightly larger than that previously reported using  
4 humic acid as the coating agent.<sup>24</sup> Formation of aggregates with no uniform size is also  
5 observed in the TEM images.  
6  
7

8 The analyses of all the interference patterns visible in the recorded images (more than  
9 50 patterns were examined) agree in evidencing the presence of magnetite in orthorhombic  
10 form ( $d_{hkl} = 4.48$  and  $2.97$  relative to (212) and (400) planes are the most common interplanar  
11 distances found, reference code 01-076-0955). Some of the patterns can be also assigned to  
12 maghemite phase. It is the case of  $d_{hkl} = 4.29, 3.73, 2.78, 2.51$  relative to (105), (203), (216),  
13 (119) planes of maghemite (reference code: 00-025-1402), but the same patterns can be  
14 assigned with almost good agreement to planes (220), (222), (314), (216) of orthorhombic  
15 magnetite phase.  
16  
17

18 The XRD pattern was used to identify the iron oxide phases of all the samples  
19 obtained from solutions of different SBO concentration (Figure S2, Supporting information).  
20 All the peak positions at  $30.1$  (220),  $35.4$  (311),  $43.0$  (400),  $53.9$  (422)  $57.2$  (511) and  $62.6$   
21 ( $440$ ) are consistent with the standard X-ray data for the magnetite phase (card number 11-  
22 0614, ICDD Database). The small signal evidenced at  $2\theta = 44.6$  could be assigned to a small  
23 amount of ferrite phase (110 plane, card number 6-0696) whose formation could occurs  
24 randomly during the synthetic procedure. We did not observe any other iron oxide peaks in  
25 the diffraction pattern of the samples. For the calculus of the particle size, the diffraction  
26 peaks corresponding to (311), (511) and (440) magnetite planes were used. The average  
27 particle diameter estimated using Scherrer formula for each sample was:  $12.2 \pm 0.2$  nm  
28 (NP/0.05),  $12.2 \pm 0.3$  nm (NP/0.1) and  $10.7 \pm 1.0$  nm (NP/0.5). These results show that the  
29 concentration of SBO employed in the synthesis does not significantly affect the size of the  
30 nanoparticles, in agreement with TEM measurements. Also, the particle sizes estimated by  
31 Scherrer equation are quite close to the TEM results (see above), indicating that the core of  
32 the nanoparticles are formed by single crystals.  
33  
34

35 To evaluate the thermal stability of the magnetite in the NPs, XRD diffraction patterns  
36 were recorded on NP/0.5, NP/0.1 and NP/0.05 samples previously heated to  $800$  °C under  $N_2$   
37 atmosphere (Figure S3, Supporting information). These analyses revealed that the magnetite  
38 was almost completely converted into hematite after the thermal treatment in the NP/0.05 and  
39 NP/0.1 samples. However, for NP/0.5, magnetite and wüstite (FeO) were identified as crystal  
40 structures in the NP. These results indicate that the amount of SBO used in the synthesis plays  
41 an important role in the thermal stability of the magnetic NPs.  
42  
43  
44  
45  
46  
47  
48  
49  
50  
51  
52  
53  
54  
55  
56  
57  
58  
59  
60

1  
2  
3 The FTIR spectra of the SBO, bare Fe<sub>3</sub>O<sub>4</sub> nanoparticles and the magnetic  
4 nanoparticles with different amounts of SBO are shown in Figure S4, Supporting information.  
5 Magnetite was observed in the nanoparticles samples by a strong absorption at 561 and 617  
6 cm<sup>-1</sup>, which corresponds to Fe–O stretching vibration.<sup>16</sup> The bands in the range from 1700 to  
7 1300 cm<sup>-1</sup> were mainly due to stretching of carboxylic groups, while those at 1031 and 1109  
8 cm<sup>-1</sup> indicated C–O stretching of polysaccharides or polysaccharide-like substances.<sup>25-26</sup>  
9 Significant differences in the spectra bands related to carboxylic and carboxylate groups were  
10 observed between the free SBO and the NPs samples. These differences are consistent with  
11 the carboxylate anions interacting with the FeO surface.<sup>27</sup> Moreover, a strong and pointed  
12 peak at 1400 cm<sup>-1</sup> observed for the NPs samples is consistent with a carboxylate-iron  
13 stretching reported by Ou et al.<sup>25</sup> The band at 1113 cm<sup>-1</sup> that appear in the SBO-coated NPs is  
14 a typical band of organic matter adsorbed on iron oxide, which is attributed to the adsorbed  
15 carbohydrates or polysaccharide-like substances.<sup>27</sup> No significant differences in the FTIR  
16 spectra were observed among the three samples of NPs.

17  
18 Figure S5, Supporting information, shows the TGA curves obtained for the three  
19 samples of NPs synthesized with different amounts of SBO. The first weight loss (up to 150  
20 °C) is assigned to adsorbed water elimination, while the second loss (up to 450 °C) to the  
21 thermal decomposition of organic matter attached to the NPs (see Table 1 for the % of organic  
22 matter bonded to the NPs measured for each sample). For the NP/0.05 and NP/0.1 samples a  
23 third phenomenon occurs at ca. 600 °C. The formation of the peaks in the range 550-650 °C in  
24 the DTA analysis for the NP/0.05 and NP/0.1 samples (inset of Figure S5, Supporting  
25 information) allows to assign the third step to the phase change of magnetite into hematite.  
26 These results are consistent with the XRD patterns of the samples heated to 800 °C (see  
27 above). Table 1 also reports the results obtained from the isotherms of N<sub>2</sub> adsorption at 77 K  
28 for NP/0.05, NP/0.1 and NP/0.5 (Figure S6, Supporting information).

29  
30 Figures 2A and 2B show the zeta potentials ( $\zeta$ ) and the particle size ( $d_z$ ) of the bare  
31 and SBO-bonded Fe<sub>3</sub>O<sub>4</sub> nanoparticles (125 mg L<sup>-1</sup>) measured in 10<sup>-2</sup> M KCl aqueous  
32 solutions at different pHs (3 - 12, adjusted with KOH or HCl). The pH of zero point charge  
33 (pH<sub>PZC</sub>) of Fe<sub>3</sub>O<sub>4</sub> was 7.2, which is close to that reported in the literature.<sup>28</sup> The pH<sub>PZC</sub> of  
34 NP/0.05 and NP/0.5 decreased to the values of 6.8 and 3.0, respectively. Since SBO is  
35 negatively charged in the range of pH 3 - 12, the positive charge observed for NP/0.05 at pHs  
36 lower than 6.8, could be the consequence of the limited covering of the Fe<sub>3</sub>O<sub>4</sub> surface by  
37 organic matter. However, when higher amount of SBO are used (i.e., NP/0.5) a negative  
38  
39  
40  
41  
42  
43  
44  
45  
46  
47  
48  
49  
50  
51  
52  
53  
54  
55  
56  
57  
58  
59  
60



1  
2  
3 charge on the surface of the nanoparticles is observed over all the investigated pH range (3 -  
4 12), which benefits the sorption of positively charged pollutants. Also, as can be seen in  
5 Figure 2A,  $\zeta$  becomes more negative as the pH increases because of the dissociation of  
6 carboxylic and phenolic groups (see below). On the other hand, the pH dependence of  $d_z$   
7 clearly shows for the three samples a maximum value of 1300 nm at  $\text{pH}_{\text{PZC}}$ , which decreases  
8 to a value of ca. 400 nm. Over the pH range between 6 and 9 the NP/0.5 sample presents the  
9 lower apparent size, incrementing its-surface area for the adsorption of pollutants.

10  
11  
12  
13  
14  
15 Carboxylic (-COOH) and phenolic (-OH) functional group contents measured by  
16 titration and their respective apparent pKa values for free SBO and the different NPs samples  
17 are shown in Table 2. The value 1.80 of the ratio -COOH/-OH obtained for this SBO is  
18 similar to that found for other type of SBO<sup>12</sup> and lower than the reported (3.2) for commercial  
19 humic acids.<sup>29-30</sup> Although both, carboxylic and phenolic groups may complex Fe ions, the  
20 smaller -COOH/-OH ratio found for NPs ( $0.13 \pm 0.03$ ) suggests that a significant fraction of  
21 the carboxylic groups of the SBO may be bonded to the magnetite surface, as also supported  
22 by the lower content of COOH groups. A similar result was found for the binding of humic  
23 acids to magnetite nanoparticles.<sup>24</sup> On the other hand, both carboxylic and phenolic group  
24 contents increase with the amount of SBO used in the synthesis. The higher values of  
25 phenolic group contents found in the NPs samples compared to free SBO indicate that, during  
26 the synthesis of the NPs, the SBO undergoes a chemical process, in which the SBO is  
27 hydroxylated by the oxidizing medium (pH  $\sim$  12 and 90 °C). The lower phenolic pKa values  
28 of the SBO bonded to the magnetite nanoparticles can be explained by the incorporation of  
29 hydroxyl groups in the aromatic rings during the synthesis procedure. The resulting poly-  
30 hydroxylated phenols are more acidic than the mono-hydroxylated phenols due to resonance  
31 stabilization of the negative charge of the unprotonated species.<sup>31</sup>

32  
33  
34  
35  
36  
37  
38  
39  
40  
41  
42  
43 Figure 3A reports the magnetization curves obtained for the three NPs. At 300 K, all  
44 samples exhibited superparamagnetic characteristics, including zero coercivity and  
45 remanence. The saturation magnetization ( $M_s$ ) of the magnetite nanoparticles synthesized  
46 with different amounts of SBO were 67 (NP/0.05), 65 (NP/0.1) and 51 (NP/0.5)  $\text{emu g}^{-1}$ . This  
47 trend is consistent with the different amount of magnetite per g of sample (i.e. 0.95, 0.90 and  
48 0.85 for NP/0.05, NP/0.1 and NP/0.5, respectively). Also, the decrease of the  $M_s$  for all the  
49 samples compared to the bulk magnetite ( $92 \text{ emu g}^{-1}$ ) is often observed with the nanoparticles  
50 and is most likely attributed to the existence of organic coating agents.<sup>32</sup> Some studies  
51 suggested that the presence of the coating agents decreases the uniformity due to quenching of  
52  
53  
54  
55  
56  
57  
58  
59  
60

1  
2  
3 surface moments, resulting in the reduction of magnetic moment in such nanoparticles.<sup>33</sup>  
4 Although higher amounts of SBO (higher covering) decrease the  $M_s$  values of the NPs, for the  
5 three samples the separation of the NPs from its aqueous dispersions can be easily completed  
6 in a few minutes with permanent hand-held magnets (Figure 3B). The dried samples are  
7 magnetically stable for a very long period of time (they were monitored for a period of two  
8 and half years); in water suspension form they are stable for a period of at least six months.  
9  
10  
11  
12  
13

#### 14 *Application of NPs as nanoadsorbent for crystal violet removal*

15  
16 Crystal violet (CV) was used to evaluate the adsorption capacity of the NPs. Sorption  
17 took place rapidly, within the first 30 min, but to be sure to reach sorption equilibrium the  
18 samples were taken for 3 h in contact with CV. The effect of the three different adsorbents on  
19 the CV removal at neutral pH was evaluated (Figure 4A). The highest % CV removal was  
20 found for the NP/0.5 (ca. 85 %) as expected considering the zeta potential measurements  
21 (Figure 2A), i.e. the high negative charge measured at the surface of the NP/0.5 at pH 7 favors  
22 sorption of the cationic dye. Figure 4B shows the increase of the adsorption capacity of  
23 NP/0.5 with increasing concentration of the adsorbent up to a CV removal of 95% at 1000 mg  
24 L<sup>-1</sup>.  
25  
26  
27  
28  
29  
30

31 The equilibrium isotherms for the adsorption of CV on NP/0.5 at pH 7 and 25 °C are  
32 shown in Figure 5 for adsorbent concentrations of 150 and 1000 mg L<sup>-1</sup>. Under both  
33 conditions, the adsorption data were fitted by Freundlich sorption model (eq. 1 reported in  
34 linearized form).  
35  
36  
37  
38

$$39 \log Q_e = \log K_f + (1/n) \log C_e \quad (1)$$

40  
41  
42 where  $Q_e$  is the sorbed CV concentration on the solid (mol g<sup>-1</sup>),  $C_e$  is the equilibrium CV  
43 concentration (mol L<sup>-1</sup>), and  $K_f$  and  $n$  are constants at a given temperature. The value of  $K_f$   
44 is indicative of the affinity adsorptive/adsorbent and  $1/n$  is an experimentally determined  
45 constant. Fitting our data to equation 1 yielded in both cases linear relationships with  $R^2$   
46 greater than 0.98 (Inset of Figure 5). Freundlich parameters for sorption ( $K_f$  and  $n$ ) calculated  
47 from the slope and intercept of the linear regression are listed in Table S1 in the Supporting  
48 information. The difference observed in the Freundlich parameters at low and high  
49 concentrations of NP/0.5 can be assigned to the higher aggregation of the nanoparticles  
50 expected for the 1000 mg/L series of experiments. There is no contradiction between this  
51  
52  
53  
54  
55  
56  
57  
58  
59  
60

1  
2  
3 result and those obtained from Figure 4B, since the isotherms reflect the amount of CV  
4 adsorbed per g of NPs. Aggregation causes a decrease in the active surface area of the  
5 adsorbent and thus seems to be a significant parameter that rules out the sorption capacity of  
6 the dye. Similar observation have been made with iron-containing hydroxyapatite  
7 nanoparticles used for the removal of  $\text{Cu}^{2+}$ .<sup>34</sup>

8  
9  
10  
11 The effect of the medium pH on the CV removal with NP/0.5 was studied by  
12 performing sorption experiments over the pH range: 3 – 10. Values of pH higher than 10 were  
13 not studied to avoid the hydrolysis of CV.<sup>35</sup> The sorption of CV on the surface of the NP/0.5  
14 is significantly influenced by the pH (Figure 6). The % CV removal increases as the pH  
15 increases up to pH 10 in agreement with the change of  $\zeta$  and  $d_z$  with pH. On the other hand,  
16 the ionic strength effect on the sorption of CV was evaluated by the addition of different  
17 amounts of NaCl. Experiments performed at pH 7, with  $[\text{CV}]_0 = 10 \text{ mg L}^{-1}$ ,  $[\text{NP}/0.5]_0 = 150$   
18  $\text{mg L}^{-1}$  and  $[\text{NaCl}]_0 = 0.005 - 0.1 \text{ M}$ , showed that the sorption of CV is not affected by the  
19 presence of NaCl (data not shown). Evidently, CV exhibits greater selectivity toward the  
20 sorbent and is not displaced by the salt and the addition of NaCl under the tested conditions  
21 do not affect significantly the aggregation of the NPs, which is important for applications to  
22 real wastewaters. Similar results were obtained by Janos<sup>36</sup> who studied the cationic dyes  
23 removal with iron humate.

24  
25  
26  
27  
28  
29  
30  
31  
32  
33 We clearly demonstrate that SBO, a bio-based product isolated from urban solid  
34 wastes, can be easily transformed into a low-cost magnetic nanoadsorbent employing a simple  
35 co-precipitation method. Further research on the adsorption of other variety of pollutants (e.g.  
36 heavy metals) and the recyclability of these NPs is still needed in order to evaluate the  
37 potential of this material for the large-scale removal of pollutants from wastewaters.

## 38 39 40 41 42 43 44 45 **ACKNOWLEDGMENTS**

46 This research was supported by ANPCyT, Argentina (PICT 2008 No. 00686),  
47 CONICET and CICIPBA, Argentina, by European Union (PIRSES-GA-2010-269128,  
48 EnvironBOS) and by Ministero delle Politiche Agricole e Forestali for the Agrienergia  
49 project. The authors are also thankful to the following institutions: (a) Acea Pinerolese Spa in  
50 Pinerolo (TO) for supplying the biobased substances sourcing materials; (b) Studio Chiono ed  
51 Associati in Rivarolo Canavese (TO) for making available pilot equipment and services for  
52  
53  
54  
55  
56  
57  
58  
59  
60

the production of the biobased substances. L.G.G., M.C.G. and L.C. are researchers from CONICET. D.O.M. is a researcher from CICPBA.

## SUPPORTING INFORMATION

Figures S1-S6 and Table S1. This information is available free of charge via the Internet at <http://pubs.acs.org/>.

## REFERENCES

- (1) Tong, D. S.; Zhou, C. H.; Lu, Y.; Yu, H.; Zhang, G. F.; Yu, W. H. Adsorption of Acid Red G dye on octadecyl trimethylammonium montmorillonite. *Appl. Clay Sci.* **2010**, *50*, 427-431.
- (2) Ghorai, S.; Sarkar, A. K.; Panda, A. B.; Pal, S. Effective removal of Congo red dye from aqueous solution using modified xanthan gum/silica hybrid nanocomposite as adsorbent. *Bioresour. Technol.* **2013**, *144*, 485-491.
- (3) Bailey, S. E.; Olin, T. J.; Bricka, R. M.; Adrian, D. D. A review of potentially low-cost sorbents for heavy metals. *Water Res.* **1999**, *33*, 2469-2479.
- (4) Lim, A. P.; Aris, A. Z. A review on economically adsorbents on heavy metals removal in water and wastewater. *Rev. Environ. Sci. Biotechnol.* **2013**, 1-19.
- (5) Crini, G. Non-conventional low-cost adsorbents for dye removal: A review. *Bioresour. Technol.* **2006**, *97*, 1061-1085.
- (6) Wan Ngah, W. S.; Hanafiah, M. A. K. M. Removal of heavy metal ions from wastewater by chemically modified plant wastes as adsorbents: A review. *Bioresour. Technol.* **2008**, *99*, 3935-3948.
- (7) Putra, E. K.; Pranowo, R.; Sunarso, J.; Indraswati, N.; Ismadji, S. Performance of activated carbon and bentonite for adsorption of amoxicillin from wastewater: Mechanisms, isotherms and kinetics. *Water Res.* **2009**, *43*, 2419-2430.
- (8) Khattri, S. D.; Singh, M. K. Removal of malachite green from dye wastewater using neem sawdust by adsorption. *J. Hazard. Mater.* **2009**, *167*, 1089-1094.
- (9) Avetta, P.; Bella, F.; Bianco Prevot, A.; Laurenti, E.; Montoneri, E.; Arques, A.; Carlos, L. Waste cleaning waste: Photodegradation of monochlorophenols in the presence of waste-derived photosensitizer. *ACS Sustainable Chem. Eng.* **2013**, *1*, 1545-1550.

- 1  
2  
3 (10) Boffa, V.; Perrone, D. G.; Montoneri, E.; Magnacca, G.; Bertinetti, L.; Garlasco, L.;  
4 Mendichi, R. A waste-derived biosurfactant for the preparation of templated silica powders.  
5 *ChemSusChem* **2010**, *3*, 445-452.  
6  
7  
8 (11) Magnacca, G.; Laurenti, E.; Vigna, E.; Franzoso, F.; Tomasso, L.; Montoneri, E.;  
9 Boffa, V. Refuse derived bio-organics and immobilized soybean peroxidase for green  
10 chemical technology. *Process Biochem.* **2012**, *47*, 2025-2031.  
11  
12 (12) Montoneri, E.; Boffa, V.; Savarino, P.; Perrone, D. G.; Musso, G.; Mendichi, R.;  
13 Chierotti, M. R.; Gobetto, R. Biosurfactants from urban green waste. *ChemSusChem* **2009**, *2*,  
14 239-247.  
15  
16  
17 (13) Gomis, J.; Bianco Prevot, A.; Montoneri, E.; González, M. C.; Amat, A. M.; Mártire,  
18 D. O.; Arques, A.; Carlos, L. Waste sourced bio-based substances for solar-driven wastewater  
19 remediation: Photodegradation of emerging pollutants. *Chem. Eng. J.* **2014**, *235*, 236-243.  
20  
21 (14) Carlos, L.; García Einschlag, F. S.; González, M. C.; Mártire, M. O. In *Waste Water -*  
22 *Treatment Technologies and Recent Analytical Developments*; García Einschlag, F. S., Ed.;  
23 InTech. ISBN: 978-953-51-0882-5: 2013.  
24  
25  
26 (15) Montoneri, E.; Mainero, D.; Boffa, V.; Perrone, D. G.; Montoneri, C. Biochemenergy:  
27 A project to turn an urban wastes treatment plant into biorefinery for the production of  
28 energy, chemicals and consumer's products with friendly environmental impact. *Int. J. Global*  
29 *Environ. Issues* **2011**, *11*, 170-196.  
30  
31 (16) Maity, D.; Agrawal, D. C. Synthesis of iron oxide nanoparticles under oxidizing  
32 environment and their stabilization in aqueous and non-aqueous media. *J. Magn. Magn.*  
33 *Mater.* **2007**, *308*, 46-55.  
34  
35 (17) Panneerselvam, P.; Morad, N.; Tan, K. A. Magnetic nanoparticle (F<sub>3</sub>O<sub>4</sub>) impregnated  
36 onto tea waste for the removal of nickel(II) from aqueous solution. *J. Hazard. Mater.* **2011**,  
37 *186*, 160-168.  
38  
39 (18) Peng, L.; Qin, P.; Lei, M.; Zeng, Q.; Song, H.; Yang, J.; Shao, J.; Liao, B.; Gu, J.  
40 Modifying Fe<sub>3</sub>O<sub>4</sub> nanoparticles with humic acid for removal of Rhodamine B in water. *J.*  
41 *Hazard. Mater.* **2012**, *209-210*, 193-198.  
42  
43 (19) Fan, L.; Luo, C.; Sun, M.; Li, X.; Lu, F.; Qiu, H. Preparation of novel magnetic  
44 chitosan/graphene oxide composite as effective adsorbents toward methylene blue. *Bioresour.*  
45 *Technol.* **2012**, *114*, 703-706.  
46  
47  
48  
49  
50  
51  
52  
53  
54  
55  
56  
57  
58  
59  
60

- 1  
2  
3 (20) Asad, S.; Amoozegar, M. A.; Pourbabae, A. A.; Sarbolouki, M. N.; Dastgheib, S. M.  
4 M. Decolorization of textile azo dyes by newly isolated halophilic and halotolerant bacteria.  
5 *Bioresour. Technol.* **2007**, *98*, 2082-2088.  
6  
7 (21) Au, W.; Pathak, S.; Collie, C. J.; Hsu, T. C. Cytogenetic toxicity of gentian violet and  
8 crystal violet on mammalian cells in vitro. *Mutat. Res.* **1978**, *58*, 269-276.  
9  
10 (22) Gomis, J.; Vercher, R. F.; Amat, A. M.; Mártire, D. O.; González, M. C.; Bianco  
11 Prevot, A.; Montoneri, E.; Arques, A.; Carlos, L. Application of soluble bio-organic  
12 substances (SBO) as photocatalysts for wastewater treatment: Sensitizing effect and photo-  
13 Fenton-like process. *Catal. Today* **2013**, *209*, 176-180.  
14  
15 (23) Hunter, R. J. Zeta potential in colloid science. Principles and applications *Academic*  
16 *Press, London* **1988**.  
17  
18 (24) Carlos, L.; Cipollone, M.; Soria, D. B.; Sergio Moreno, M.; Ogilby, P. R.; García  
19 Einschlag, F. S.; Mártire, D. O. The effect of humic acid binding to magnetite nanoparticles  
20 on the photogeneration of reactive oxygen species. *Sep. Purif. Technol.* **2012**, *91*, 23-29.  
21  
22 (25) Ou, X.; Chen, S.; Quan, X.; Zhao, H. Photochemical activity and characterization of  
23 the complex of humic acids with iron(III). *J. Geochem. Explor.* **2009**, *102*, 49-55.  
24  
25 (26) Celi, L.; Lamacchia, S.; Marsan, F. A.; Barberis, E. Interaction of inositol  
26 hexaphosphate on clays: Adsorption and charging phenomena. *Soil Science* **1999**, *164*, 574-  
27 585.  
28  
29 (27) Gu, B.; Schmitt, J.; Chen, Z.; Liang, L.; McCarthy, J. F. Adsorption and desorption of  
30 natural organic matter on iron oxide: Mechanisms and models. *Environ. Sci. Technol.* **1994**,  
31 *28*, 38-46.  
32  
33 (28) Chang, Y. C.; Chen, D. H. Preparation and adsorption properties of monodisperse  
34 chitosan-bound Fe<sub>3</sub>O<sub>4</sub> magnetic nanoparticles for removal of Cu(II) ions. *J. Colloid Interface*  
35 *Sci.* **2005**, *283*, 446-451.  
36  
37 (29) Gao, K.; Pearce, J.; Jones, J.; Taylor, C. Interaction between peat, humic acid and  
38 aqueous metal ions. *Environ. Geochem. Health* **1999**, *21*, 13-26.  
39  
40 (30) Ritchie, J. D.; Michael Perdue, E. Proton-binding study of standard and reference  
41 fulvic acids, humic acids, and natural organic matter. *Geochim. Cosmochim. Acta* **2003**, *67*,  
42 85-93.  
43  
44 (31) Mukherji, S. M.; Singh, S. P.; Kapoor, R. P.; Dass, R. Organic Chemistry Vol. II. *New*  
45 *Age International Publishers, New York* **2012**.  
46  
47  
48  
49  
50  
51  
52  
53  
54  
55  
56  
57  
58  
59  
60

- 1  
2  
3 (32) Sun, X.; Zheng, C.; Zhang, F.; Yang, Y.; Wu, G.; Yu, A.; Guan, N. Size-controlled  
4 synthesis of magnetite (Fe<sub>3</sub>O<sub>4</sub>) nanoparticles coated with glucose and gluconic acid from a  
5 single Fe(III) precursor by a sucrose bifunctional hydrothermal method. *J. Phys. Chem.* **2009**,  
6 *113*, 16002-16008.  
7  
8  
9 (33) Kim, D. K.; Mikhaylova, M.; Zhang, Y.; Muhammed, M. Protective coating of  
10 superparamagnetic iron oxide nanoparticles. *Chem. Mater.* **2003**, *15*, 1617-1627.  
11  
12 (34) Mercado, D. F.; Magnacca, G.; Malandrino, M.; Rubert, A.; Montoneri, E.; Celi, L.;  
13 Bianco Prevot, A.; Gonzalez, M. C. Paramagnetic Iron-Doped Hydroxyapatite Nanoparticles  
14 with Improved Metal Sorption Properties. A Bioorganic Substrates-Mediated Synthesis. *ACS*  
15 *Appl. Mater. Interfaces* **2014**, *6*, 3937-3946.  
16  
17 (35) Arias-Estevez, M.; Astray, G.; Cid, A.; Fernández-Gándara, D.; García-Río, L.;  
18 Mejuto, J. C. Influence of colloid suspensions of humic acids upon the alkaline fading of  
19 carbocations. *J. Phys. Org. Chem.* **2008**, *21*, 555-560.  
20  
21 (36) Janoš, P. Sorption of Basic Dyes onto Iron Humate. *Environ. Sci. Technol.* **2003**, *37*,  
22 5792-5798.  
23  
24  
25  
26  
27  
28  
29  
30  
31  
32  
33  
34  
35  
36  
37  
38  
39  
40  
41  
42  
43  
44  
45  
46  
47  
48  
49  
50  
51  
52  
53  
54  
55  
56  
57  
58  
59  
60

1  
2  
3  
4  
5  
6  
7  
8  
9  
10  
11  
12  
13 **Tables and Figures**  
14  
15

16 **Table 1.** Apparent specific surface areas and SBO amounts bonded to the NPs surface.  
17

Sample	Specific Surface Area <sup>a</sup> (m <sup>2</sup> g <sup>-1</sup> )	SBO adsorbed to Fe <sub>3</sub> O <sub>4</sub> <sup>b</sup> (%)
NP/0.5	35	~15
NP/0.1	55	~10
NP/0.05	63	~5

26 <sup>a</sup> BET model; <sup>b</sup> TGA analysis.  
27  
28  
29  
30  
31  
32

33 **Table 2.** Mean concentration values of groups with apparent pKa on the acid side (carboxylic  
34 groups) and with pKa on the basic side (phenol groups).  
35

Sample	-COOH (mmol.g <sup>-1</sup> )	pKa <sub>1</sub>	Ph-OH (mmol.g <sup>-1</sup> )	pKa <sub>2</sub>	Total acidity (mmol.g <sup>-1</sup> )
SBO	1.40 ± 0.20	6.6 ± 0.1	0.78 ± 0.07	10.2 ± 0.1	2.1 ± 0.2
NP/0.05	0.13 ± 0.11	6.3 ± 0.3	0.91 ± 0.09	9.3 ± 0.2	1.0 ± 0.2
NP/0.1	0.21 ± 0.15	6.3 ± 0.1	1.3 ± 0.4	9.2 ± 0.1	1.5 ± 0.6
NP/0.5	0.25 ± 0.18	6.5 ± 0.1	2.8 ± 0.1	9.2 ± 0.1	3.0 ± 0.3

48  
49 Confidence interval between replicates of 95%.  
50  
51  
52  
53  
54  
55  
56  
57  
58  
59  
60



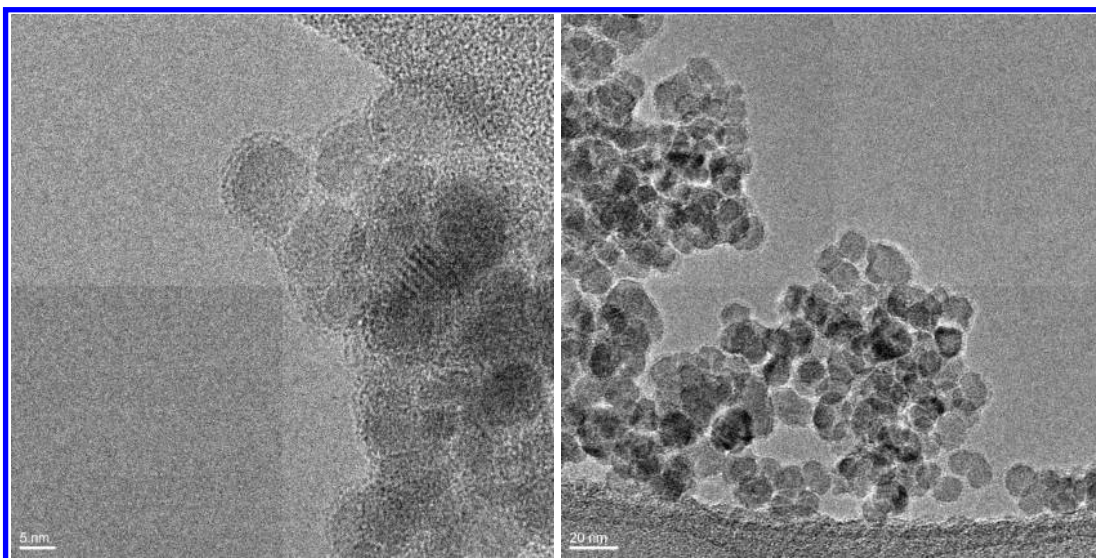


**Figure 1.** HR-TEM images of NP/0.5.

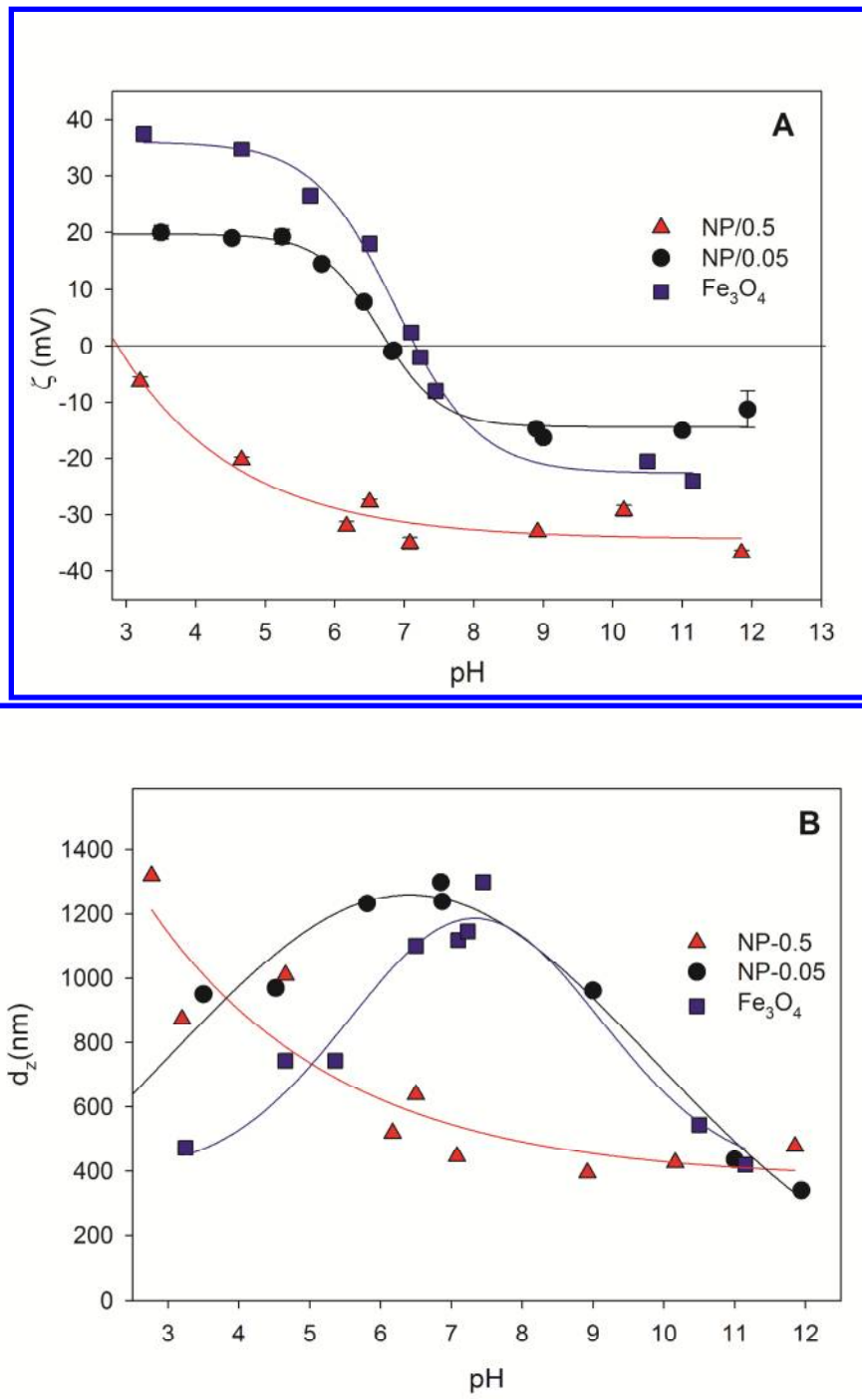
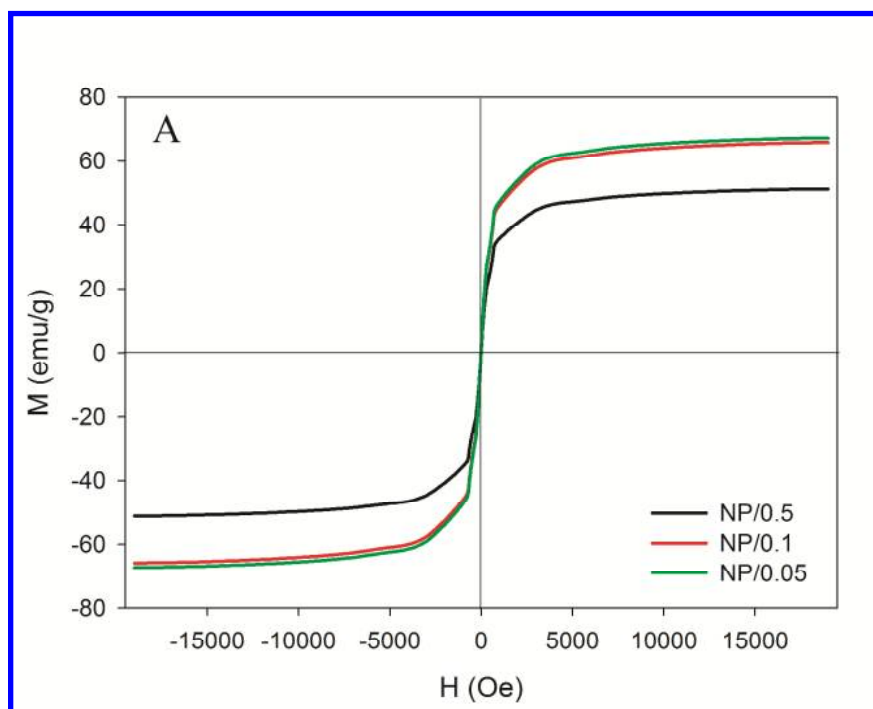


**Figure 2.** Variation of (A) zeta potentials ( $\zeta$ ) and (B) the particle size ( $d_z$ ) of naked magnetite ( $\text{Fe}_3\text{O}_4$ ), NP/0.05 and NP/0.5 as a function of pH in 0.01 M KCl.



45  
46  
47  
48  
49  
50  
51  
52  
53  
54  
55  
56  
57  
58  
59  
60

**Figure 3.** A) Magnetization curves of NP/0.5, NP/0.1 and NP/0.05 at 300 K. B) NP/0.5 dispersed in aqueous-solution and magnetic separation.

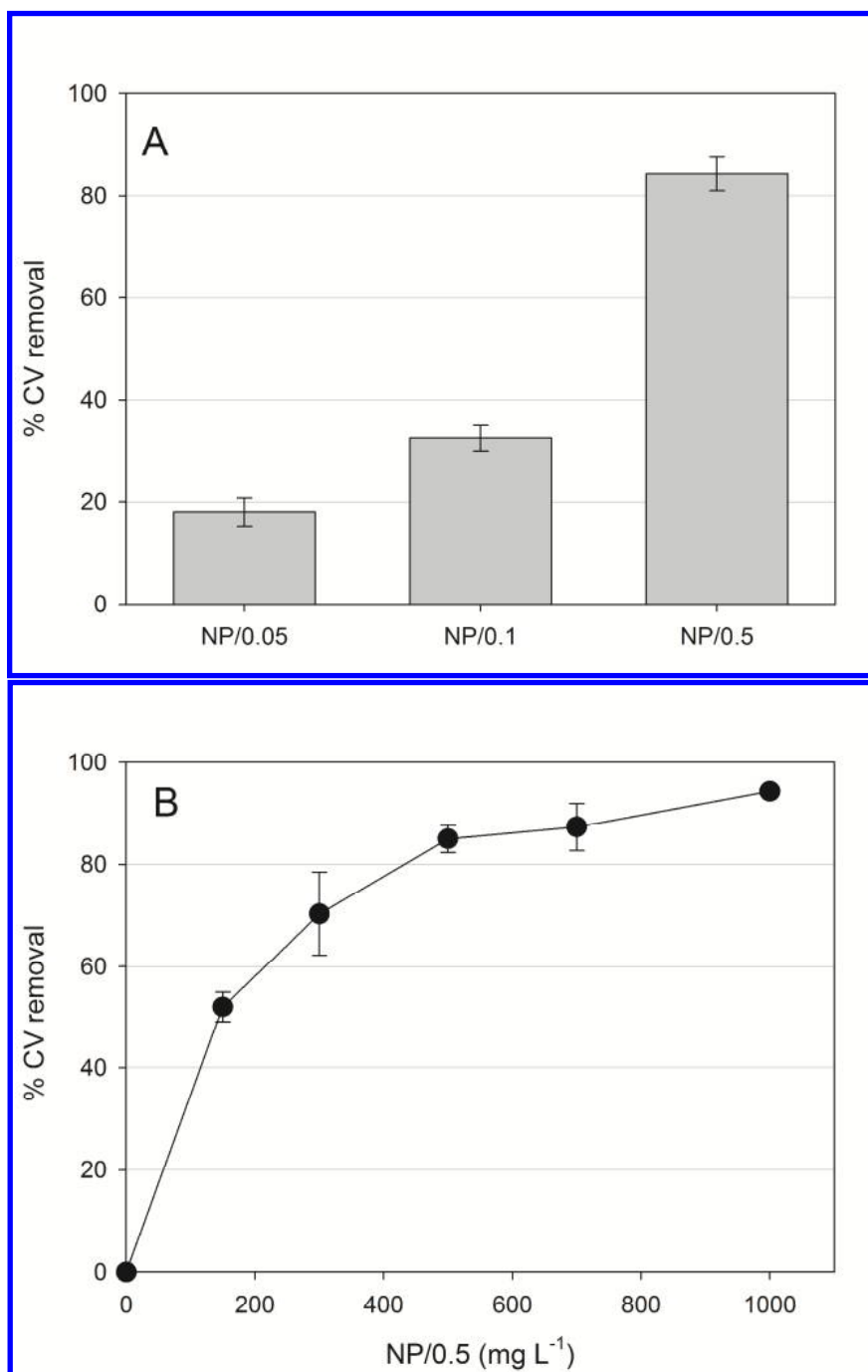


**Figure 4.** A) CV removal obtained with NPs prepared with different amounts of SBO.  $[CV]_0 = 10 \text{ mg L}^{-1}$ ;  $[NP]_0 = 500 \text{ mg L}^{-1}$ ;  $\text{pH} = 7$ ,  $T = 25 \pm 2 \text{ }^\circ\text{C}$ . B) The effect of NP/0.5 dosage on the adsorption of CV.  $[CV]_0 = 10 \text{ mg/L}$ ,  $\text{pH} = 7$ ,  $T = 25 \pm 2 \text{ }^\circ\text{C}$ . The error bars represent the standard deviation of the data obtained by triplicate.

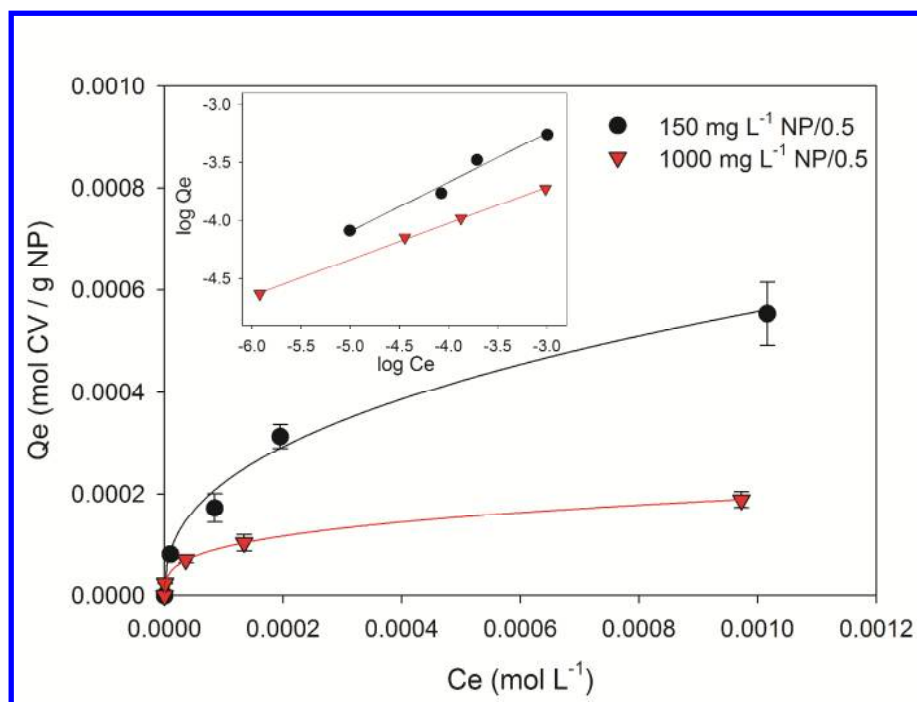


**Figure 5.** Adsorption isotherms of CV on NP/0.5 obtained at pH = 7 and  $25 \pm 2$  °C with different NP/0.5 concentrations ( $150 \text{ mg L}^{-1}$  and  $1000 \text{ mg L}^{-1}$ ). The error bars represent the standard deviation of the data obtained by triplicate. Inset: logarithmic plot of the data according to Freundlich linearized model (eq. 1).

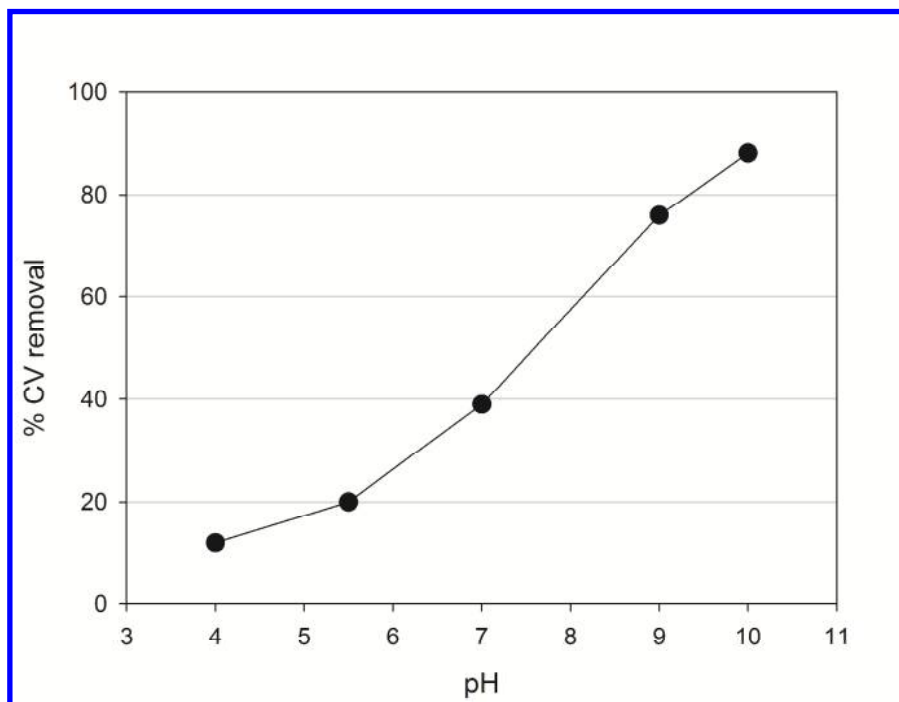


**Figure 6.** CV removal obtained with NP/0.5 at different pHs.  $[CV]_0 = 10 \text{ mg L}^{-1}$ ;  $[NP/0.5]_0 = 150 \text{ mg L}^{-1}$ .

### For Table of Contents Use Only

Novel magnetite nanoparticles coated with waste sourced bio-based substances as sustainable and renewable adsorbing materials

Giuliana Magnacca, Alex Allera, Enzo Montoneri, Luisella Celi, Damián E. Benito, Leonardo G. Gagliardi, Mónica C. Gonzalez, Daniel O. Mártire and Luciano Carlos\*

### Synopsis

Preparation and characterization of magnetite nanoparticles coating with a bio-based product isolated from urban solid wastes, and its application as low-cost magnetic nanoadsorbents for the removal of crystal violet is discussed.

### TOC/Abstract art

